European Radiology (2019) 29:4008–4015
https://doi.org/10.1007/s00330-018-5829-9

COMPUTER APPLICATIONS

CT reconstruction algorithms affect histogram and texture analysis: evidence for liver parenchyma, focal solid liver lesions, and renal cysts

Su Joa Ahn[1] · Jung Hoon Kim[1,2] · Sang Min Lee[3] · Sang Joon Park[1] · Joon Koo Han[1,2]

Received: 13 March 2018 / Revised: 20 September 2018 / Accepted: 12 October 2018 / Published online: 19 November 2018

Abstract

Purpose To determine the effects of different reconstruction algorithms on histogram and texture features in different targets.

Materials and methods Among 3620 patients, 480 had normal liver parenchyma, 494 had focal solid liver lesions (metastases = 259; hepatocellular carcinoma = 99; hemangioma = 78; abscess = 32; and cholangiocarcinoma = 26), and 488 had renal cysts. CT images were reconstructed with filtered back-projection (FBP), hybrid iterative reconstruction (HIR), and iterative model reconstruction (IMR) algorithms. Computerized histogram and texture analyses were performed by extracting 11 features.

Results Different reconstruction algorithms had distinct, significant effects. IMR had a greater effect than HIR. For instance, IMR had a significant effect on five features of liver parenchyma, nine features of focal liver lesions, and four features of renal cysts on portal-phase scans and four, eight, and four features, respectively, on precontrast scans ($p < 0.05$). Meanwhile, different algorithms had a greater effect on focal liver lesions (six in HIR and nine in IMR on portal-phase, three in HIR, and eight in IMR on precontrast scans) than on liver parenchyma or cysts. The mean attenuation and standard deviation were not affected by the reconstruction algorithm ($p > .05$). Most parameters showed good or excellent intra- and interobserver agreement, with intraclass correlation coefficients ranging from 0.634 to 0.972.

Conclusions Different reconstruction algorithms affect histogram and texture features. Reconstruction algorithms showed stronger effects in focal liver lesions than in liver parenchyma or renal cysts.

Key Points

- *Imaging heterogeneities influenced the quantification of image features.*
- *Different reconstruction algorithms had a significant effect on histogram and texture features.*
- *Solid liver lesions were more affected than liver parenchyma or cysts.*

Keywords Liver · Kidney · Cyst · Neoplasms · Tomography

Abbreviations

ASM	Angular second moment
FBP	Filtered back-projection
GLCM	Gray level co-occurrence matrix
HIR	Hybrid iterative reconstruction
ICC	Intraclass correlation coefficient
IDM	Inverse difference moment
IMR	Iterative model reconstruction
PACS	Picture archiving and communications system
ROI	Region of interest

Electronic supplementary material The online version of this article (https://doi.org/10.1007/s00330-018-5829-9) contains supplementary material, which is available to authorized users.

✉ Jung Hoon Kim
jhkim2008@gmail.com

[1] Department of Radiology, Seoul National University Hospital, 101 Daehangno, Jongno-gu, Seoul 110-744, Republic of Korea

[2] Department of Radiology and Institute of Radiation Medicine, Seoul National University College of Medicine, 101 Daehang-no, Chongno-gu, Seoul 110-744, Korea

[3] Department of Radiology, Hallym University Sacred Heart Hospital, 22, Gwanpyeong-ro 170beon-gil, Anyang-si 431-796, Korea

Introduction

Noninvasive, quantitative, imaging-based biomarkers are expected to make major contributions to personalized medicine. Quantitative image features extracted from CT and MR imaging have been investigated for a variety of oncology applications, in particular for predicting the prognosis and assessing the patient response to targeted therapies [1–3]. However, most of the

studies analyze existing image data sets obtained retrospectively. These studies often consist of heterogeneous image data acquired from various scanners using different scanning techniques and reconstruction algorithms. For this reason, as there is limited clinical application of the results, it is important to consider the reproducibility, standardization, and quality control obtained during the process of developing imaging biomarkers.

Among imaging biomarkers, texture analysis is emerging as a useful technique for assessing the tumor heterogeneity determined during routine clinical practice and without any additional data acquisition [4, 5]. Clinical studies have indicated the ability of CT texture analysis to provide independent predictors of survival for patients with lung cancer, esophageal cancer, colorectal cancer, or head and neck cancer and its ability to be an early marker of the treatment response in metastatic renal cancer [5].

Several iterative reconstruction methods have been proposed for reducing the radiation dose by decreasing image noise during the reconstruction process while maintaining the diagnostic quality [6, 7]. The number of CT examinations has increased owing to technical advances and the wide availability of CT scanners. Consequently, concerns regarding the amount of patient radiation exposure and its risks have also increased [8]. In response, there have been increased demands to reduce the overall radiation dose. Most recently, an algorithm termed knowledge-based iterative model reconstruction (IMR) became the latest advance in reconstruction techniques. This technique is purported to improve image quality better than standard-dose filtered back-projection (FBP) and the hybrid iterative reconstruction (HIR) algorithm, which incorporates statistics-model-based denoising into raw and image data spaces [9, 10]. However, this is accomplished by creating unique image textures and properties that differ from those shown using the traditional algorithm [11]. To date, only a few studies have given an idea of how such imaging heterogeneities might influence the quantification of image features [12, 13].

The purpose of our study is to determine the effects of different reconstruction algorithms, including FBP, HIR, and IMR, on the computer-based histogram and texture features for liver parenchyma, focal solid liver lesions, and renal cysts from the same CT image data from a single CT scanner.

Materials and methods

Study population and design

Our institutional review board approved this retrospective study, and the requirement for informed consent was waived. We reviewed the hospital's medical records and the radiology databases. We identified 3620 patients (2032 men, 1588 women; mean age, 63.5 years; age range, 18–82 years) who underwent MDCT with a single scanner between September 2015 and March 2016. Among these patients, 2623 had no focal solid mass in the liver, 997 patients had a focal solid liver lesion, and 1486 patients had renal cysts. Among the 2623 patients who had no focal liver mass, we excluded a number of factors for analysis of normal liver parenchyma: underlying chronic liver disease ($n = 715$); a history of a malignant condition in the whole body, including the liver, such as lymphoproliferative disease or GI tract cancer ($n = 1340$); or a general inflammatory condition, such as sepsis, peritonitis, or hepatitis, that can affect liver function ($n = 88$). Among the 997 patients who had a focal solid liver lesion, we excluded simple hepatic cysts using image features such as a well-defined, round, or ovoid hypo-attenuating, unenhanced lesion [14]. We also excluded infiltrative masses ($n = 92$) and lesions smaller than 2 cm in size ($n = 411$). Among the 1486 patients who had renal cysts, we excluded renal cysts less than 2 cm ($n = 901$) and with an internal septum, mural nodule, or calcification ($n = 97$).

Finally, we included 480 patients with normal liver parenchyma (294 men, 186 women; mean age, 56 years; age range, 18–72 years), 494 patients with focal solid liver lesions (267 men, 227 women; mean age, 64 years; range, 38–78 years), and 488 patients with simple renal cysts (251 men, 237 women; mean age, 61.7 years; age range, 31–68 years). Focal solid liver lesions included hepatic metastases ($n = 259$), hepatocellular carcinoma ($n = 99$), hemangioma ($n = 78$), hepatic abscess ($n = 32$), and cholangiocarcinoma ($n = 26$). A flowchart of the overall study design is shown in Fig. 1.

Image acquisition

All studies were performed using a 64-detector row CT scanner (iCT; Philips Medical Systems) with a collimated beam width at the isocenter of 80 mm, 100 kVp, and tube current modulation (Z-DOM, ACS & D-DOM, Philips Medical Systems). For CT texture analysis, we included 494 CT scans of focal solid liver lesions and 480 CT scans of liver parenchyma. Among 488 CT images obtained for renal cyst analysis, 216 CT images were already included in the analysis of focal solid liver lesions or liver parenchyma. Finally, 1246 CT images, including 321 patients with quadruple-phase CT (precontrast, arterial, portal, and delayed phase), 280 patients with triple-phase CT (precontrast, arterial, and portal phase), 259 patients with double-phase CT (arterial and portal phases), 257 patients with double-phase CT (precontrast and portal phases), and 129 patients with single-phase CT (portal phase only) were enrolled in this study.

The CT scanning parameters were as follows: detector configuration, 0.625 mm; pitch, 0.891; rotation time, 0.75 s; 100 kVp; 130 mAs; and slice thickness/reconstruction interval, 3/3 mm; reconstruction kernel, standard. For all patients, 1.5 mL/kg of 350 mgI/mL iobitridol (Xenetix 350, Guerbet) or iohexol (Bonorex 350, CMS) was injected at a rate of 3 mL/s using an automatic power injector (Envision CT; Medrad). The pre- and

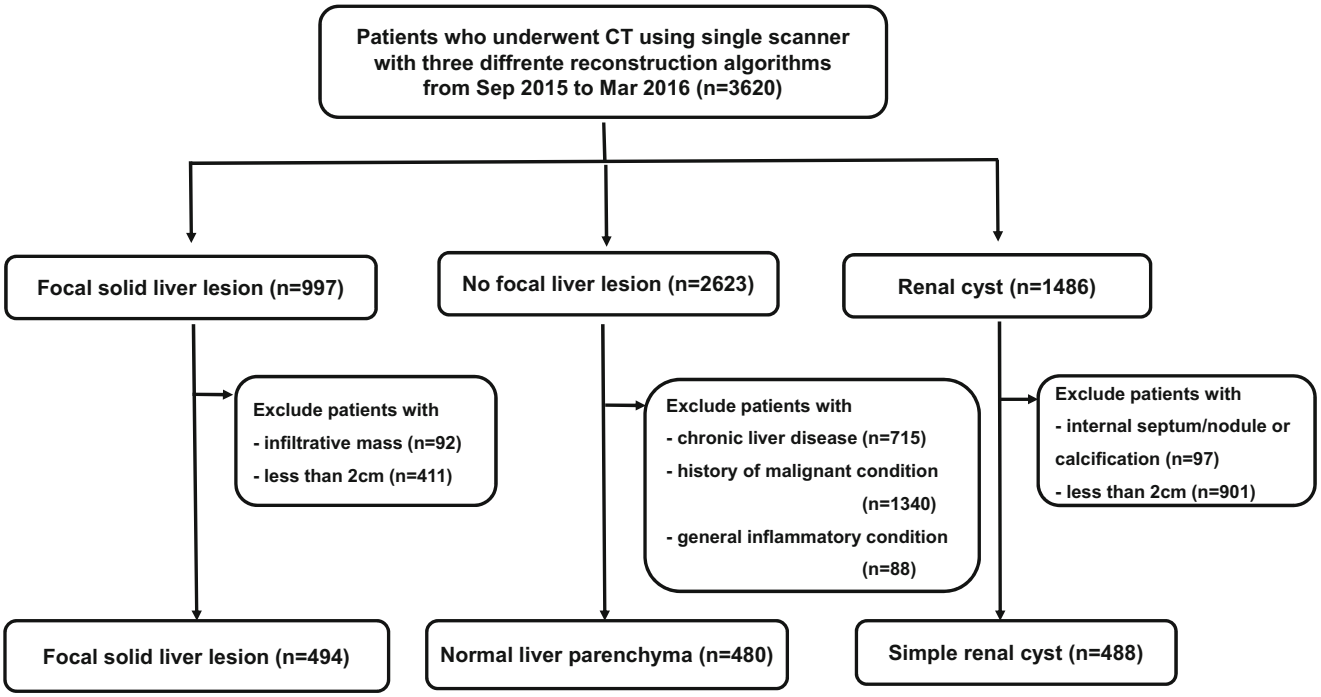

Fig. 1 Flowchart of the study group inclusion process. *Numbers in parentheses are numbers of patients. CT, computed tomography

postcontrast scans were obtained during two different breath holds. Arterial-phase imaging was performed for 19 s after obtaining 100 HU attenuation of the descending aorta measured using a bolus tracking method. A 33-s delay after the arterial phase was allowed for portal-phase acquisition. After acquisition of the portal phase, additional delayed scanning was performed on a quadruple-phase CT for 3 min following contrast agent administration. For single-phase CT, portal-phase imaging was performed 60 s after achieving 50 HU attenuation of the descending aorta, as measured using a bolus-tracking method. All images were reconstructed with a slice thickness of 3 mm by using three reconstruction algorithms, i.e., FBP, HIR, and IMR.

Computer-based extraction and analysis of quantitative features

The portal-phase CT image sets using the three different reconstruction algorithms were retrieved using a picture archiving and communications system (PACS; Maroview, version 5.4, Infinitt) and were loaded onto a standard workstation (XW6200, Hewlett-Packard) for further textural analysis. Among the 1246 CT images, 858 of them contained precontrast scans, which were also retrieved and loaded onto a standard workstation for texture analysis. For texture analysis, a personal computer–based, in-house software program (Medical Imaging Solution for Segmentation and Texture Analysis) was used for lesion segmentation with fully automated quantification of the texture features implemented using a dedicated C++ language (Microsoft Foundation Classes; Microsoft). In our study, texture analysis was initially applied to portal-phase imaging.

The reviewers consisted of two abdominal radiologists (S.J.A. with 9 years and S.M.L. with 7 years of clinical experience in abdominal imaging). Before the analysis, each assessor was provided with a summary document outlining the method of assessing each lesion. Each reviewer manually segmented the lesion on the FBP image. Afterwards, all segmentations were visually confirmed (J.H.K. with 17 years of clinical experience in abdominal imaging) and manually adjusted as needed to ensure accuracy. For evaluation of normal liver parenchyma, we selected the largest liver slice obtained at the right main portal vein level and after manual segmentation at the boundary of the liver surface. We manually removed significant-sized vessels (larger than 1 cm in diameter), including the IVC and the main portal vein. For focal solid liver lesions and renal cysts, we drew the region of interest (ROI) along the outline of the lesion to define the largest cross-sectional area (Fig. 2**)**. After confirmation of the ROI, the texture features were automatically calculated. Following analysis of the FBP image, we continually analyzed the HIR (iDose, Philips Medical Systems) and IMR images after applying the saved ROI at the same level of the slice. After finishing the analysis of the portal-phase images, we analyzed the precontrast scan using the saved ROI at the same level of the slice (Fig. 3**)**. The texture features of the precontrast scan within the ROI were automatically calculated as described above. The computerized texture analysis software program provided 11 quantitative imaging features, including histogram parameters (mean attenuation, standard deviation, skewness, kurtosis, entropy, and homogeneity) and texture parameters (gray level co-occurrence matrices (GLCM) moments, GLCM angular second moment (ASM), GLCM inverse difference moment

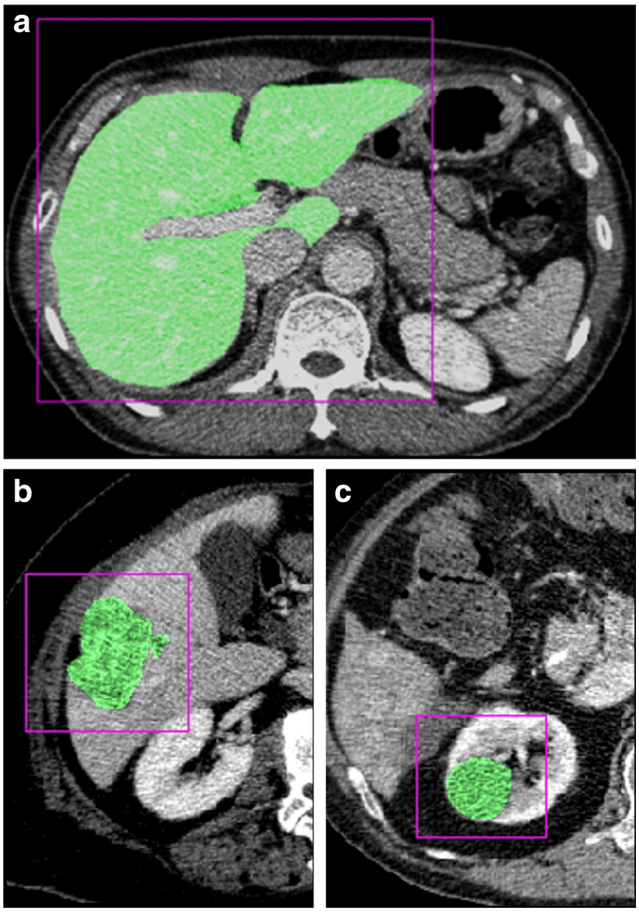

Fig. 2 CT texture analysis software program in normal liver parenchyma, focal solid liver lesion, and renal cyst. For evaluation of normal liver parenchyma (**a**), manual segmentation was done at the boundary of the liver surface at the level of the largest liver slice with the right main portal vein. After that, we removed significantly sized vessels (larger than 1 cm diameter), including the IVC and main portal vein. For focal solid liver lesions (**b**) and renal cysts (**c**), the ROI was drawn along the outline of the lesion to define the largest cross-sectional area. Next, segmentation was manually conducted, and texture features of the ROI were automatically extracted and calculated by the software program

(IDM), GLCM contrast, and GCLM entropy). At a minimum of 4 weeks after reviewing the texture analysis, the first reviewer reanalyzed the images to assess the intraobserver reliability. Each reviewer remained blinded to the other analysis results to avoid bias.

Statistical analysis

One-way analysis of variance (ANOVA) was used to ascertain the statistical significance of the difference between the three reconstruction algorithms using the mean value of the calculated texture parameters. To assess the effects of the reconstruction algorithm on the measured lesion features, the data from the quantitative lesion feature extraction were analyzed using a fitting simple linear mixed-effects model. The model was fitted using the restricted maximum likelihood with statistics software (SPSS, SPSS version 21, IBM). All of the effects were examined with respect to the reference conditions of the FBP. The results were further analyzed to determine the total number of features of the significantly affected reconstruction algorithm for each lesion type. The intra- and inter-observer reproducibilities of the texture parameters were evaluated by calculating the intraclass correlation coefficient (ICC). An ICC value below 0.40 was considered poor reliability, fair for values between 0.41 and 0.59, good for values between 0.60 and 0.74, and excellent for values between 0.75 and 1.00 [15]. *P* values below 0.05 were considered statistically significant.

Results

The effective diameter and area were 38.66 ± 32.59 mm and 969.92 ± 1823.19 mm^2, respectively, in the focal solid liver lesions, 26.87 ± 32.59 mm and 428.41 ± 1823.19 mm^2 in the renal cysts, and 239.57 ± 32.59 and 16,043.65 ± 1823.19 mm^2 in the liver parenchyma. The mean attenuation in the portal and precontrast scans revealed no significant difference in the three different reconstruction algorithms in the normal liver parenchyma, the focal solid liver lesions, and the renal cysts ($p > 0.05$). Appendices E1 and E2 summarize the histogram and texture features seen on the portal-phase and precontrast images between the different reconstruction algorithms.

Comparison of different reconstruction algorithms affecting histogram and texture features in liver parenchyma

The HIR showed a significant difference in entropy, homogeneity, and GLCM IDM compared with FBP ($p < 0.05$) in both the precontrast and portal phases. The IMR showed a significant difference in skewness, kurtosis, homogeneity, GLCM IDM, and GLCM contrast in the portal phase and in skewness, homogeneity, GLCM IDM, and GLCM entropy in the precontrast scan ($p < 0.05$). Both iterative reconstruction algorithms showed a significant difference in homogeneity and GLCM IDM compared with FBP, not only in the portal-phase but also in the precontrast scan ($p < 0.05$, Table 1).

Comparison of different reconstruction algorithms' effects on the histogram and texture features in focal solid liver lesions

The HIR showed a significant difference in entropy, homogeneity, and GLCM moments compared with the FBP ($p < 0.05$) in both the precontrast and portal phases. Skewness, kurtosis, and GLCM IDM only showed a significant difference in the portal-phase images. However, the IMR showed significant differences in skewness, kurtosis, entropy, homogeneity,

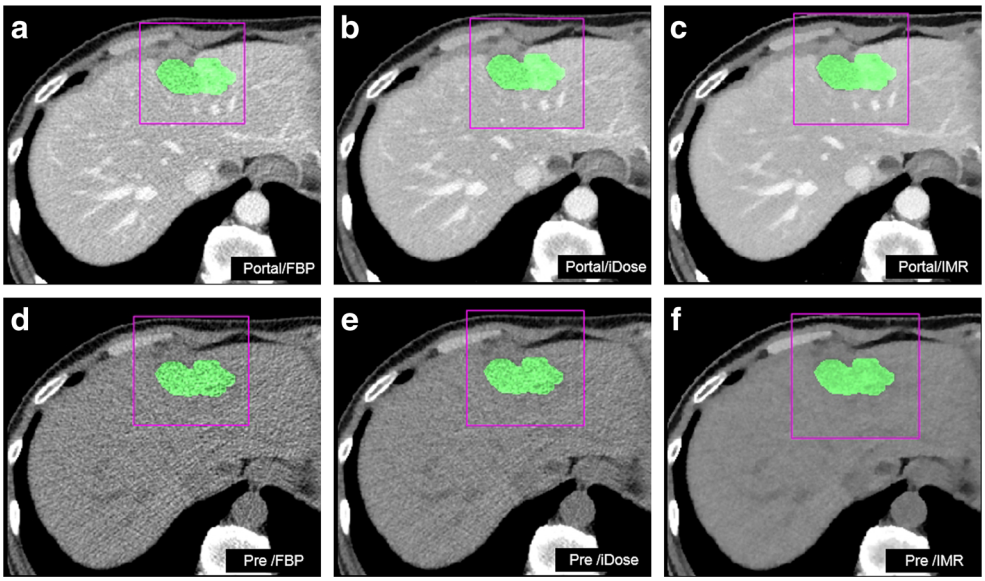

Fig. 3 CT texture analysis software program in portal-phase and precontrast scans. Texture features calculated in three different algorithms, including FBP, HIR, and IMR, in both portal-phase (**a**, **b**, **c**) and precontrast scans (**d**, **e**, **f**) using the same ROI at the same level of CT slice

GLCM moments, GLCM ASM, GLCM IDM, and GLCM entropy in both the precontrast and portal phases ($p < 0.05$). GLCM contrast was only significantly different in the portal phase. Both iterative reconstruction algorithms showed a significant difference in entropy, homogeneity, and GLCM moments compared with the FBP in both the precontrast and portal phases ($p < 0.05$, Table 2).

Comparison of different reconstruction algorithms' effects on histogram and texture features in renal cysts

The HIR showed a significant difference in entropy and homogeneity in the portal phase and entropy in precontrast images compared with FBP ($p < 0.05$). However, the IMR showed a significant difference in skewness, kurtosis, entropy, and GLCM contrast in both the precontrast and portal phases ($p < 0.05$). Both iterative reconstruction algorithms showed a significant difference in entropy compared with FBP in both the precontrast and portal phases ($p < 0.05$, Table 3).

Comparison of different reconstruction algorithms' effects on histogram and texture features

Each of the different reconstruction algorithms affected the histogram and texture features. Compared with FBP, IMR had a more significant difference than HIR. For focal solid liver lesions, IMR showed a significant difference in nine parameters in the portal phase and in eight parameters in the precontrast images. For renal cysts, IMR showed a significant difference in four values in both precontrast and portal-phase images. For normal liver parenchyma, five parameters in the portal phase and four parameters in the precontrast images showed a significant difference. Focal solid liver lesions were affected more than renal cysts or liver parenchyma in each reconstruction algorithm (Appendix E3).

Table 1 Comparison of the effect of different reconstruction algorithms for histogram and texture features in liver parenchyma

	Characteristics	Portal phase ($n = 480$)						Pre-contrast scan ($n = 412$)					
		FBP		HIR		IMR		FBP		HIR		IMR	
		Effect	*p* value	Effect	*p* value	Effect	*p* value	Effect	*p* value	Effect	*p* value	Effect	*p* value
Histogram parameters	Mean attenuation (HU)	2.14	< 0.01	0. 09	0.32	0.31	0.06	2.13	< 0.01	0. 21	0.18	0.31	0.07
	Standard deviation (HU)	3.24	< 0.01	0.03	0.07	-0.214	0.08	2.72	< 0.01	1.47	0.16	-1.06	0.06
	Skewness	0.05	0.724	0.08	0.41	0.49	0.02	1.00	0.71	0.85	0.331	0.35	0.02
	Kurtosis	1.74	0.01	0.09	0.48	0.32	< 0.01	1.44	< 0.01	0.89	0.65	0.31	0.08
	Entropy	5.54	< 0.01	-0.31	0.02	-0.18	0.08	6.15	< 0.01	-0.68	0.02	-0.01	0.16
	Homogeneity	0.45	< 0.01	0.03	0.03	0.03	0.03	1.43	< 0.01	0.12	0.03	0.11	0.04
Texture parameters	GLCM moments	0.22	< 0.01	0.18	0.51	0.21	0.11	0.21	< 0.01	0.36	0.61	0.27	0.11
	GLCM ASM	0.50	< 0.01	0.10	0.08	0.07	0.21	0.68	< 0.01	0.54	0.08	1.00	0.52
	GLCM IDM	-2.99	< 0.01	0.31	0.03	0.45	0.01	-1.24	< 0.01	0.21	0.02	0.55	0.01
	GLCM contrast	0.03	< 0.01	0.01	0.58	-0.04	0.03	0.10	< 0.01	0.03	0.42	-0.20	0.02
	GLCM entropy	-1.09	< 0.01	0.06	0.40	0.60	0.09	-2.00	< 0.01	0.01	0.27	0.71	0.21

Table 2 Comparison of the effect of different reconstruction algorithms for histogram and texture features in focal solid liver lesion

	Characteristics	Portal phase ($n = 494$)						Pre contrast scan ($n = 382$)					
		FBP		HIR		IMR		FBP		HIR		IMR	
		Effect	*p* value	Effect	*p* value	Effect	*p* value	Effect	*p* value	Effect	*p* value	Effect	*p* value
Histogram parameters	Mean attenuation (HU)	2.99	< 0.01	0.36	0.05	0.78	0.07	3.22	< 0.01	1.54	0.32	0.99	0.07
	Standard deviation (HU)	3.21	0.03	0.25	0.38	-0.33	0.08	3.14	0.10	0.56	0.24	-1.01	0.06
	Skewness	0.11	0.48	0.45	0.03	0.63	< 0.01	0.34	0.14	0.21	0.40	0.91	0.01
	Kurtosis	1.54	< 0.01	0.08	0.02	0.21	0.03	3.17	< 0.01	0.54	0.05	0.04	< 0.01
	Entropy	4.21	< 0.01	-0.22	0.04	-0.65	0.03	5.24	< 0.01	-0.52	0.03	-0.67	0.03
	Homogeneity	0.65	< 0.01	0.03	0.02	0.01	< 0.01	0.71	< 0.01	0.11	0.04	0.16	0.01
Texture parameters	GLCM moments	0.43	< 0.01	0.05	0.04	0.02	0.01	0.79	0.02	0.12	0.03	0.06	0.02
	GLCM ASM	0.57	< 0.01	0.12	0.09	0.01	0.02	0.45	< 0.01	0.24	0.41	0.01	0.04
	GLCM IDM	2.58	< 0.01	0.11	0.03	0.10	< 0.01	3.11	< 0.01	0.68	0.07	0.15	0.02
	GLCM contrast	0.10	< 0.01	0.00	0.58	-0.03	0.04	0.41	< 0.01	0.27	0.08	-0.11	0.07
	GLCM entropy	-1.21	< 0.01	1.03	0.45	0.74	0.03	-3.25	< 0.01	0.60	0.52	2.58	0.02

Inter- and intraobserver reproducibility of texture analysis

In the portal phase, the intraobserver reproducibility of the histographic and morphological parameters was excellent (ICC > 0.75), except for the GLCM contrast of IMR of liver parenchyma (ICC = 0.745). The interobserver reproducibility of the morphologic parameters of IMR was less than those of the other two reconstructions in all three lesions, i.e., GLCM contrast of liver parenchyma (ICC = 0.744), GLCM IDM (ICC = 0.634), GLCM contrast of focal solid lesions (ICC = 0.534), and GLCM moments of renal cysts (ICC = 0.534), compared to the values for GLCM ASM (ICC = 0.722) and GLCM contrast of focal solid lesions (ICC = 0.580) on FBP and GLCM entropy of focal solid lesions (ICC = 0.701) on HIR. All of the histographic and morphologic parameters obtained on precontrast scans showed excellent intraobserver and interobserver reproducibility (ICC > 0.75, Appendix E4, E5).

Discussion

Texture analysis is useful in assessing the response to cancer treatments [16–18]. However, according to previous reports, there is no clear indication as to whether different types of reconstruction algorithm can affect quantitative histogram and texture features. Our study results show that the reconstruction algorithms can significantly affect many quantitative histogram and texture features. Different reconstruction algorithms showed more effects in focal liver lesions than in liver parenchyma or renal cysts. In addition, IMR had a stronger effect than HIR. Therefore, the effect of different reconstruction algorithms should be considered when using histogram and texture analysis, especially for IMR or solid lesions.

Even though the FBP technique is the most widely used CT reconstruction algorithm, this technique has major drawbacks, as it assumes noiseless projection data, resulting in image noise. With the advancement of CT techniques, such as marked reduction in noise, new iterative reconstruction algorithms are being

Table 3 Comparison of the effect of different reconstruction algorithms for histogram and texture features in renal cyst

	Characteristics	Portal phase ($n = 488$)						Pre contrast scan ($n = 364$)					
		FBP		HIR		IMR		FBP		HIR		IMR	
		Effect	*p* value	Effect	*p* value	Effect	*p* value	Effect	*p* value	Effect	*p* value	Effect	*p* value
Histographic parameters	Mean attenuation (HU)	1.17	< 0.01	0. 31	0.17	0.22	0.47	2.10	< 0.01	0.11	0.07	0.37	0.06
	Standard deviation (HU)	2.45	< 0.01	-0.01	0.07	-0.04	0.09	1.98	< 0.01	1.10	0.74	-0.10	0.07
	Skewness	0.10	0.50	0.21	0.40	0.64	0.01	0.09	0.45	0.12	0.71	1.12	0.02
	Kurtosis	1.01	< 0.01	0.25	0.45	0.06	< 0.01	0.74	< 0.01	0.45	0.09	0.12	0.02
	Entropy	5.14	< 0.01	-0.41	0.03	-0.38	0.04	5.14	0.01	-0.45	0.04	-0.48	0.04
	Homogeneity	0.48	< 0.01	0.02	0.04	0.23	0.07	0.45	0.02	0.07	0.05	0.08	0.06
Morphologic parameter	GLCM moments	0.27	< 0.01	0.21	0.65	0.35	0.54	0.44	< 0.01	0.34	0.09	0.07	0.05
	GLCM ASM	0.50	< 0.01	0.30	0.47	0.01	0.21	0.49	< 0.01	0.09	0.07	0.21	0.35
	GLCM IDM	-3.20	< 0.01	1.21	0.45	1.40	0.31	-2.21	< 0.01	0.15	0.41	0.10	0.07
	GLCM contrast	0.02	< 0.01	0.01	0.58	-0.02	0.01	0.11	< 0.01	0.09	0.60	-0.41	0.03
	GLCM entropy	-1.04	< 0.01	0.07	0.47	0.59	0.08	-0.02	0.60	0.04	0.32	0.61	0.09

developed to improve image quality while preserving the resolving power for visualization of fine details [19]. Most recently, an algorithm known as knowledge-based IMR became the latest advancement in CT reconstruction techniques. HIR incorporates statistics-model-based denoising into raw and image data space, and these techniques are replacing FBP as the standard of CT reconstruction [20]. Compared to FBP, for instance, IMR produces reduced image noise and artifacting, as IMR is a more advanced statistical noise model and a more detailed model of the MDCT system [21]. The IMR technique is claimed to improve image quality. Two published clinical studies have reported dose reduction and image quality improvements using IMR [22, 23]. Given the differences between algorithms and the resulting reconstructed images, they create unique image textures and properties, differing from those using traditional FBP algorithms [11]. To date, a few studies have been published on how such imaging heterogeneities might influence the quantification of image features. Recent investigations suggest that these factors may influence the quantitative measurements [12]. Solomon et al [13] also showed that the reconstruction algorithms affect the quantitative imaging features in liver lesions, lung nodules, and renal stones on MDCT. These results are consistent with our results. However, there have been no prominent studies regarding the effects of the different reconstruction algorithms on texture analysis according to the lesion component. In our study, focal liver lesions showed a more significant effect than liver parenchyma or renal cysts in different reconstruction algorithms. CT texture analysis is one approach for quantifying spatial heterogeneity by extracting data of the pixel spatial intensity variations across a tissue of interest. In general, we expect that a pure cyst may be less affected than a heterogeneous solid lesion in a reconstruction algorithm by visual assessment and texture analysis. However, texture analysis has been frequently applied to focal solid lesions. We should be aware that focal solid lesions showed a more significant effect than liver parenchyma or renal cysts in different reconstruction algorithms.

Accumulated data have shown that texture-analyzed features are important for determining invisible structural changes and the biological heterogeneity of a lesion [24–26]. However, before applying the texture-analyzed features for specific diseases, we should understand the technical factors that affect the texture analysis. Our results demonstrate how changing reconstruction algorithms on MDCT can affect the quantitative texture parameters. We should be aware that if images obtained in different reconstruction techniques are being considered, potential differences in analyzed features that occur in the same lesion may not be due to real change in the disease progression. Not only the reconstruction algorithm but also other CT parameters, such as tube voltage, tube current, and detector configuration, may affect the quantitative texture features. Future investigations should determine whether these different CT parameters affect texture analysis features.

Our study has several limitations. First, as the study only considers a limited number of patients, our research may have a potential selection bias. Second, as the texture features in this study were derived from the results of manual segmentation by a radiologist, these results can be significantly influenced by a subjective tendency. However, we used the same ROI in the different reconstruction algorithms. Nonetheless, we believe that a reliable and robust automatic boundary extraction method should be further developed to address the variability issue. Third, all of the comparisons made were relative to FBP, and the data address the differences in the texture feature measurements between reconstruction methods, not the precision of these features. To assess their accuracy, a reference standard must be known. In addition, because not all texture parameters are independent, we need to further evaluate the relationships between all the different histogram and texture parameters. In future work, radiologists should characterize the precision of the texture feature measurements using phantom or hybrid CT datasets with practical embedded lesions [27]. Additionally, in comparison to FBP, we have assessed only two iterative reconstruction methods from a single vendor. With different reconstruction settings, future studies may identify further effects on the quantitative imaging features of lesions.

In conclusion, our study results show that the reconstruction algorithms can significantly affect many quantitative histogram and texture features. Different reconstruction algorithms showed more effects in focal liver lesions than in liver parenchyma or renal cysts.

Acknowledgments We thank Bonnie Hami, M.A. (USA), for her editorial assistance in the preparation of this manuscript.

Funding The authors state that this work has not received any funding.

Compliance with ethical standards

Guarantor The scientific guarantor of this publication is Joon Koo Han, M.D.

Conflict of interest The authors of this manuscript declare no relationships with any companies, whose products or services may be related to the subject matter of the article.

Statistics and biometry Su Joa Ahn, MD, has significant statistical expertise and no complex statistical methods were necessary for this paper.

Informed consent Written informed consent was waived by the Institutional Review Board.

Ethical approval Institutional Review Board approval was obtained (IRB No. 1706–128-861).

Methodology
- Retrospective
- Diagnostic or prognostic study
- Performed at one institution

References

1. Castellano G, Bonilha L, Li LM, Cendes F (2004) Texture analysis of medical images. Clin Radiol 59:1061–1069
2. Gevaert O, Xu J, Hoang CD et al (2012) Non-small cell lung cancer: identifying prognostic imaging biomarkers by leveraging public gene expression microarray data–methods and preliminary results. Radiology 264:387–396
3. Choi CM, Kim MY, Lee JC, Kim HJ (2014) Advanced lung adenocarcinoma harboring a mutation of the epidermal growth factor receptor: CT findings after tyrosine kinase inhibitor therapy. Radiology 270:574–582
4. Davnall F, Yip CS, Ljungqvist G et al (2012) Assessment of tumor heterogeneity: an emerging imaging tool for clinical practice? Insights Imaging 3:573–589
5. Ganeshan B, Miles KA (2013) Quantifying tumour heterogeneity with CT. Cancer Imaging 13:140–149
6. Scheffel H, Stolzmann P, Schlett CL et al (2012) Coronary artery plaques: cardiac CT with model-based and adaptive-statistical iterative reconstruction technique. Eur J Radiol 81:e363–e369
7. Singh S, Kalra MK, Do S et al (2012) Comparison of hybrid and pure iterative reconstruction techniques with conventional filtered back projection: dose reduction potential in the abdomen. J Comput Assist Tomogr 36:347–353
8. Berrington de González A, Mahesh M, Kim KP et al (2009) Projected cancer risks from computed tomographic scans performed in the United States in 2007. Arch Intern Med 169:2071–2077
9. Hu MQ, Li M, Liu ZY, Huang MP, Liu H, Liang CH (2016) Image quality evaluation of iterative model reconstruction on low tube voltage (80 kVp) coronary CT angiography in an animal study. Acta Radiol 57:170–177
10. Nakaura T, Iyama Y, Kidoh M et al (2016) Comparison of iterative model, hybrid iterative, and filtered back projection reconstruction techniques in low-dose brain CT: impact of thin-slice imaging. Neuroradiology 58:245–251
11. Schulz B, Beeres M, Bodelle B et al (2013) Performance of iterative image reconstruction in CT of the paranasal sinuses: a phantom study. AJNR Am J Neuroradiol 34:1072–1076
12. Barrett HH, Myers KJ, Hoeschen C, Kupinski MA, Little MP (2015) Task-based measures of image quality and their relation to radiation dose and patient risk. Phys Med Biol 60:R1–R75
13. Solomon J, Mileto A, Nelson RC, Roy Choudhury K, Samei E (2016) Quantitative features of liver lesions, lung nodules, and renal stones at multi-detector row CT examinations: dependency on radiation dose and reconstruction algorithm. Radiology 279:185–194
14. Mortelé KJ, Ros PR (2001) Cystic focal liver lesions in the adult: differential CT and MR imaging features. Radiohgraphics 21:895–910
15. Chalian H, Tochetto SM, Töre HG, Rezai P, Yaghmai V (2012) Hepatic tumors: region-of-interest versus volumetric analysis for quantification of attenuation at CT. Radiology 262:853–861
16. Ahn SJ, Kim JH, Park SJ, Han JK (2016) Prediction of the therapeutic response after FOLFOX and FOLFIRI treatment for patients with liver metastasis from colorectal cancer using computerized CT texture analysis. Eur J Radiol 85:1867–1874
17. Chee CG, Kim YH, Lee KH et al (2017) CT texture analysis in patients with locally advanced rectal cancer treated with neoadjuvant chemoradiotherapy: a potential imaging biomarker for treatment response and prognosis. PLoS One 12:e0182883
18. Haider MA, Vosough A, Khalvati F, Kiss A, Ganeshan B, Bjarnason GA (2017) CT texture analysis: a potential tool for prediction of survival in patients with metastatic clear cell carcinoma treated with sunitinib. Cancer Imaging 17:4
19. Löve A, Olsson ML, Siemund R, Stålhammar F, Bjorkman-Burtscher IM, Söderberg M (2013) Six iterative reconstruction algorithms in brain CT: a phantom study on image quality at different radiation dose levels. Br J Radiol 86:20130388
20. Marin D, Choudhury KR, Gupta RT et al (2013) Clinical impact of an adaptive statistical iterative reconstruction algorithm for detection of hypervascular liver tumours using a low tube voltage, high tube current MDCT technique. Eur Radiol 23:3325–3335
21. Brown KM, Zabic S, Koehler T (2012) Acceleration of ML iterative algorithms for CT by the use of fast start images. Physics of Medical Imaging. https://doi.org/10.1117/12.911412
22. Oda S, Utsunomiya D, Funama Y et al (2014) A knowledge-based iterative model reconstruction algorithm: can super-low-dose cardiac CT be applicable in clinical settings? Acad Radiol 21:104–110
23. Suchá D, Willemink MJ, de Jong PA et al (2014) The impact of a new model-based iterative reconstruction algorithm on prosthetic heart valve related artifacts at reduced radiation dose MDCT. Int J Cardiovasc Imaging 30:785–793
24. Miles KA, Ganeshan B, Griffiths MR, Young RC, Chatwin CR (2009) Colorectal cancer: texture analysis of portal phase hepatic CT images as a potential marker of survival. Radiology 250:444–452
25. Ng F, Kozarski R, Ganeshan B, Goh V (2013) Assessment of tumor heterogeneity by CT texture analysis: can the largest cross-sectional area be used as an alternative to whole tumor analysis? Eur J Radiol 82:342–348
26. Ozkan E, West A, Dedelow JA et al (2015) CT gray-level texture analysis as a quantitative imaging biomarker of epidermal growth factor receptor mutation status in adenocarcinoma of the lung. AJR Am J Roentgenol 205:1016–1025
27. Solomon J, Samei E (2014) A generic framework to simulate realistic lung, liver and renal pathologies in CT imaging. Phys Med Biol 59:6637–6657